Nanoscale

Accepted Manuscript

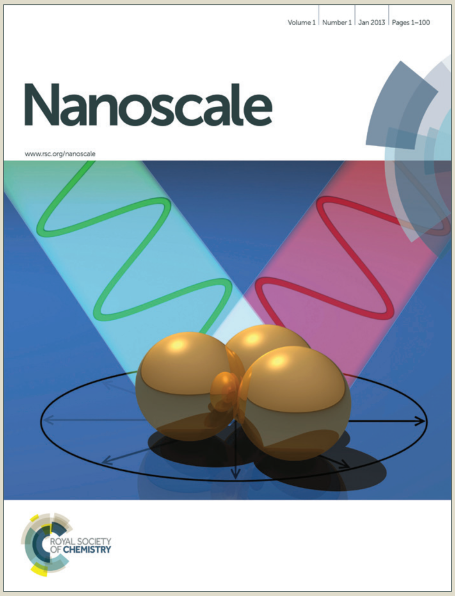

ROYAL SOCIETY OF CHEMISTRY

www.rsc.org/nanoscale

Integrating Biologically Inspired Nanomaterials and Table-top Stereolithography for 3D Printed Biomimetic Osteochondral Scaffolds

Nathan J. Castro[1], Joseph O'Brien[2] and Lijie Grace Zhang[1, 3, 4*]

[1]Department of Mechanical and Aerospace Engineering, The George Washington University, Washington DC 20052, USA

[2]Departments of Orthopedic Surgery & Neurological Surgery, The George Washington University, Washington, DC 20052, USA

[3]Department of Biomedical Engineering, The George Washington University, Washington DC 20052, USA

[4]Department of Medicine, The George Washington University, Washington DC 20052, USA

*Corresponding Author:

Dr. Lijie Grace Zhang

Tel: 202-994-2479

Fax: 202-994-0238

Email: lgzhang@gwu.edu

Mailing Address: 3590 Science and Engineering Hall, 800 22nd Street NW, Washington DC, 20052

Abstract

The osteochondral interface of an arthritic joint is notoriously difficult to regenerate due to its extremely poor regenerative capacity and complex stratified architecture. Native osteochondral tissue extracellular matrix is composed of numerous nanoscale organic and inorganic constituents. Although various tissue engineering strategies exist in addressing osteochondral defects, limitations persist with regards to tissue scaffolding which exhibit biomimetic cues at the nano to micro scale. In an effort to address this, the current work focused on 3D printing biomimetic nanocomposite scaffolds for improved osteochondral tissue regeneration. For this purpose, two biologically-inspired nanomaterials have been synthesized consisting of (1) osteoconductive nanocrystalline hydroxyapatite (nHA) (primary inorganic component of bone) and (2) core-shell poly(lactic-co-glycolic) acid (PLGA) nanospheres encapsulated with chondrogenic transforming growth-factor β1 (TGF-β1) for sustained delivery. Then, a novel table-top stereolithography 3D printer and the nano-ink (i.e., nHA + nanosphere + hydrogel) were employed to fabricate a porous and highly interconnected osteochondral scaffold with hierarchical nano-to-micro structure and spatiotemporal bioactive factor gradients. Our results showed that human bone marrow-derived mesenchymal stem cell adhesion, proliferation, and osteochondral differentiation were greatly improved in the biomimetic graded 3D printed osteochondral construct *in vitro*. The current work served to illustrate the efficacy of the nano-ink and current 3D printing technology for efficient fabrication of a novel nanocomposite hydrogel scaffold. In addition, tissue-specific growth factors illustrated a synergistic effect leading to increased cell adhesion and directed stem cell differentiation.

Keywords: Nanobiomaterials, 3D printing, stem cells, stereolithography, osteochondral

Introduction

Recent advancements in the area of tissue engineering and the development of porous three-dimensional (3D) implantable scaffolds for tissue regeneration have placed a greater demand on the need for novel biomaterials which exhibit bioactive properties, as well as lend themselves to be tunable and modifiable for tissue-specific applications. Traditional methodologies such as porogen leaching[1-3] and gas foaming[4, 5] have been extensively studied and employed in the fabrication of porous scaffolds, but several limitations exist; namely, the lack of control of uniform pore dispersion, pore geometry, pore size, and interconnectivity,[6-9] all of which are necessary for successful integration of the 3D scaffold and host tissue.[10-12] More advanced scaffold fabrication techniques such as the twin-screw extrusion system used by Erisken et al.[13, 14], Ozkan et al.[15, 16], and Ergun et al.[17, 18] have addressed some of these limitations while also focusing on spatially controlled incorporation of tissue-specific morphogenetic factors for enhanced and directed cell behavior. Another promising strategy which has been applied towards this research area is 3D bioprinting.

3D bioprinting technologies provide an efficient means of addressing the aforementioned limitations of traditional scaffold fabrication methods by allowing for precise control and placement of biomaterials, cells, and bioactive factors within a pre-designed natural or synthetic 3D tissue matrix.[19, 20] With the development of novel biomaterials tailored to a specific 3D printing technology, tissue-specific 3D scaffolds with desirable chemical and mechanical properties can be readily manufactured. One such 3D printing technology which has garnered greater attention for use in the manufacture of bioactive 3D scaffolds is stereolithography (SL).[21, 22] SL can be used to manufacture 3D scaffolds for tissue regeneration applications due its capability of producing highly accurate 3D parts. The 3D scaffold can be created by polymerizing and/or photocrosslinking a liquid resin via ultraviolet (UV) light resulting in solidification of the liquid resin in a layer-by-layer process yielding a pre-designed 3D architecture. SL printing has shown the capacity of higher resolution, more accuracy, and precise control of 3D internal and external architecture than many other techniques. Unfortunately, constraints related to costs and maintenance of commercial systems have limited their wide access to research laboratories. Therefore, one aim of the current work was to develop a table-top stereolithography system capable of resolving features akin to industrial systems for the fabrication of multi-material bioactive scaffolds for osteochondral regeneration.

In addition to manufacturing constraints, a dearth of 3D printable bioinks with biomimetic nanoscale features for SL and other 3D bioprinting systems exists. An ideal bioink for 3D bioprinting should satisfy several essential criteria. Firstly, it should be biocompatible, bioactive and biomimetic for maximal cell growth and tissue integration. Secondly, they should be employable within various 3D bioprinting platforms. Unfortunately, only few available synthetic and natural biomaterials have shown to be suitable for 3D bioprinting to include: poly(ethylene glycol) (PEG) and derivatives, collagen, hyaluronic acid, and others.[23, 24] It is still particularly challenging to fabricate highly biomimetic tissue constructs based on current available biomaterials while regulating transplanted or native cell population(s) for efficient tissue regeneration. In fact, the native osteochondral extracellular matrix (ECM), is structurally hierarchical and nanocomposite in nature.[25] Nanobiomaterials, a research area at the forefront of nanotechnology and biomaterials, are designed to resemble cellular microenvironment components and regulate cell behavior, which are currently having a profound impact on the field of tissue regeneration.[25] However, current nanobiomaterials for 3D bioprinting of functional osteochondral tissue are extremely limited.[19]

Therefore, the main objective of this study is to develop biologically-inspired nanomaterials to be used as a series of bioinks for the fabrication of biomimetic graded osteochondral scaffolds via a novel table-top SL system. Two bioactive nanomaterials were synthesized in this study: one is hydrothermally treated nanocrystalline hydroxyapatite (nHA)[26-30] which can not only serve as a nano mechanical reinforcer, but also as an osteoconductive factor due to its biomimetic structure and composition. The other nanomaterial is a core-shell poly(lactic-co-glycolic) acid (PLGA) nanosphere encapsulated with chondrogenic transforming growth-factor β1 (TGF-β1) via a coaxial electrospraying technique. The core-shell nanospheres aim to serve as a controlled growth factor delivery system for sustained TGF-β1 delivery. The selected PLGA has excellent biocompatibility, mechanical properties, and a slower degradation rate, rendering it ideal for controlled growth factor delivery. Coaxial electrospraying[31] enables the separation of organic and aqueous phases and thus allows for effective incorporation of biologically active components such as growth factors into the aqueous phase with no exposure to harmful organic solvents.

Figure 1 shows the overall design of the study. With the use of computer-aided design (CAD) software and table-top SL printing, bioactive biomimetic scaffolds were fabricated containing a gradient of nHA within the highly porous subchondral bone layer and chondrogenic TGF-β1 nanospheres in the cartilage layer for enhanced osteochondral regeneration. The following experimental groups were tested: a three layer scaffold (2 bone layers/ 1 cartilage layer) (-nHA / -TGF-β1) served as a control alongside the following experimental groups "graded" (+20% and 10% nHA / -TGF-β1), "blended" (+20% and 10% nHA / +bare TGF-β1), and "spheres" (+20% and 10% nHA / +TGF-β1 nanospheres). The effectiveness of incorporating spatiotemporal nanomaterials and growth factor cues for directed human bone marrow derived mesenchymal stem cell (hMSC) adhesion, growth, chondrogenic and osteogenic differentiation was explored *in vitro*. The proposed work also illustrates the capacity of our table-top SL printer in fabricating physiologically relevant nanocomposite scaffolds.

Experimental

Development of a table-top SL printer

Printer design and cure depth assessment: The novel table top SL apparatus was developed based on the existing Solidoodle® 3D printer platform for use as a desktop SL system for additive manufacturing of nanomaterials. Open source software (Prontrface®) was employed to control the 3 stepper motors with an effective resolution of 100 µm in x, y, and z-axis. The major modification to the existing platform is the incorporation of a 110 µm fiber optic-coupled solid-state UV (355 nm) laser (MarketTech, Scotts Valley, CA). Per the manufacturer's specifications, the effective spot size of the emitted light is 190 ± 50 µm with an energy output of ~20 uJ at 15 kHz. A glass petri dish was fixed upon the print bed to function as a minivat for the addition of liquid photocurable resin. Due to the ability to alter the frequency of the pulsed signal, power at the material's surface can be controlled with a range ~40-110 mW.

A 60% wt/wt polyethylene glycol diacrylate (PEG-Da, Mn = 700) in PEG (Mw = 300) hydrogel solution was selected as a bulk printing matrix material to characterize cure depth of the printer and used for the incorporation of tissue-specific nanomaterials in all studies. A photoinitiator, Bis(2,4,6-trimethylbenzoyl)-phenylphosphineoxide (BAPO) (BASF, Florham Park, NJ), with excitation in the ultraviolet (UV) range was added to the PEG:PEG-Da mixture at 0.5 wt% of PEG-Da and allowed to rest overnight for adequate dissolution. Specifically, the hydrogel solution was pipetted inside a plastic petri dish filled up to the rim. A glass slide was placed on top of the container, in contact with the solution. The glass slide acted as a substrate that allowed the gel to adhere to the underside of the glass slide during laser exposure thus facilitating the measurement of the solidified gel. Samples were cured by activating the laser and drawing a line at various print speeds through the glass slide and into the PEG-Da photopolymer solution. After polymerization, the glass slide was lifted off the petri dish containing the adhered polymerized gel. The cured gels were rinsed with distilled water to remove unreacted PEG-Da, and the thickness (in z) of the gels was then measured with a micrometer. Five gels were cured for each of the PEG-Da solutions, and the average thickness was determined.

Hydrothermally treated nHA and TGF-β1 encapsulated PLGA core-shell nanospheres synthesis

nHA synthesis: A wet chemistry plus hydrothermal treatment method was used to synthesize nHA with good crystallinity and nanometer particle size as described in our previous papers [32-36]. Briefly, 37.5 mL of a 0.6 M ammonium phosphate (Sigma Aldrich, St. Louis, MO) solution was added to 375 mL of water and adjusted to pH 10 with ammonium hydroxide (Fisher Scientific, Pittsburgh, PA). A 1 M calcium nitrate (Sigma Aldrich, St. Louis, MO) solution added dropwise into the above mixture while stirring. Precipitation of HA continued for 10 min at room temperature. Upon complete addition of calcium nitrate, the HA precipitate containing solution was hydrothermally treated at 200 °C for 20 h in a 125 mL Teflon liner (Parr Instrument Company, Moline, IL). After 20 h, the nHA precipitate was centrifuged and rinsed thoroughly with water three times, dried at 80 °C for 12 h and ground into a fine powder.

TGF-β1 encapsulated core-shell nanosphere fabrication: Poly(lactic-*co*-glycolic) acid (PLGA) (Lactel Absorbable Polymers, Birmingham, AL) nanospheres were fabricated by coaxial wet electrospray via a custom coaxial needle system. The coaxial system consisted of a 26 G core needle (304SS 0.018” OD, 0.01”ID) receded within a 20G shell needle (304SS 0.036” OD, 0.0275” ID) (McMaster-Carr, Robbinsville, NJ 08691). Specifically, TGF-β1 (PeproTech, Rocky Hill, New Jersey) lyophilized powder was resuspended per manufacturer’s instructions (10 ng/mL) and used in all experiments. For TGF-β1 encapsulated nanospheres, a 2.5 wt% solution of PLGA in acetone (Sigma-Aldrich, St. Louis, MO) was fed through the shell feed inlet at a flow rate of 4.0 mL/hour. TGF-β1 was fed through the core feed inlet at the same flow rate. Voltage was adjusted during collection to prevent fiber formation and maintain adequate Taylor cone morphology. PLGA nanospheres were collected in an ultrapure water stabilizing bath. After collection, the bath was transferred to a centrifuge tube and ultrasonicated for 30 seconds (Ultrasonicator, QSonica, Newtown, CT). Emulsified samples were then immediately frozen and lyophilized for 24 hours to remove the stabilizing bath prior to use. Transmission electron microscopy (TEM, JEOL 1200 EX) was employed for morphological examination and size analysis of the two synthesized nanomaterials.

Bioactive graded osteochondral scaffold fabrication

3D scaffold design and printing: A series of 15 mm × 1.2 mm solid disks with predesigned architecture were designed in Rhinoceros3D (McNeel North America, Seattle, Washington), prepared for 3D printing using the open source software package Slic3r, and fabricated via our table-top SL printer. The previously characterized PEG-Da:PEG mixture was used for all experiments. Specifically, 3 mL of the hydrogel solution was added to a rigid glass petri dish fixed upon the print bed and allowed to dwell for 2 minutes. The volume used produced an effective layer thickness of 400 µm. For hMSC adhesion and proliferation studies, bare hydrogel scaffolds with increasing in-fill density (40%, 60%, and 80%) which corresponds to the solid fraction of each printed layer were fabricated. Then, graded osteochondral scaffolds were fabricated with nHA concentrations of 20% and 10% of PEG-Da for the porous osseous layer and transitional calcified cartilage layer. Furthermore, a solid cartilage layer containing either bare TGF-β1 (10 ng/mL) or TGF-β1 encapsulated nanospheres of equivalent concentration were added to PEG-Da:PEG mixture for enhanced chondrogenesis. Fabricated samples were rinsed in ultrapure water and allowed to swell overnight for dissolution of the soluble PEG fraction. Upon swelling, a 5 mm biopsy punch was used to collect cylindrical samples. Scaffold morphology was examined via scanning electron microscopy (SEM, Zeiss NVision 40 FIB) at 3 kV accelerating voltage.

TGF-β1 release study: Two week TGF-β1 release profiles in the scaffolds containing bare TGF-β1 or TGF-β1 encapsulated nanospheres were evaluated. Briefly, 5 mm of the above two types of scaffolds (n=3) were incubated in phosphate-buffered saline (PBS) at 37°C. Fractions of the supernatant were collected after 4, 24, 72 hours, 1 and 2 weeks, respectively and TGF-β1 content was measured spectrophotometrically (Multiskan GO® Spectrophotometer, Thermo Scientific, Waltham, MA) via a TGF-β1 enzyme-linked immunosorbent assay (ELISA). Growth factor release profiles were plotted as a fraction of total encapsulated growth factor.

Mechanical testing: The compressive elastic modulus of the 3D printed scaffolds was determined via uniform compression testing (n=5) (Applied Test Systems, Butler, PA) fitted with a 100 N load cell at a crosshead speed of 5 mm/min. 5 mm samples were placed in ultrapure water and allowed to swell for 24 hours with intermittent exchange of fresh ultrapure water and blotted dry prior to testing. Load and displacement were used to plot the stress-strain curves and the Young's modulus was calculated from the linear elastic region.

hMSC in vitro studies

Primary hMSCs were obtained from healthy consenting donors from the Texas A&M Health Science Center, Institute for Regenerative Medicine. The cells (passage #3-6) were cultured in complete media composed of Alpha Minimum Essential medium (α-MEM, Gibco, Grand Island, NY) supplemented with 16.5% fetal bovine serum (Atlanta Biologicals, Lawrenceville, GA), 1% (v/v) L-Glutamine (Invitrogen, Carlsbad, CA), and 1% penicillin:streptomycin (Invitrogen, Carlsbad, CA) and cultured under standard cell culture conditions (37°C, a humidified, 5% CO_2/95% air environment). All 3D printed samples were sterilized in 70% ethanol for 30 min then washed 3 times for 5 min in PBS before cell seeding.

hMSC adhesion and proliferation: Porous multilayer scaffolds of increasing in-fill density were evaluated for hMSC adhesion. Specifically, hMSCs were seeded at 50,000 cells/scaffold. Seeded scaffolds were incubated under standard cell culture conditions for 4 hours. After rinsing with PBS, the adherent cells were lifted enzymatically and quantified via MTS assay (CellTiter 96® AQueous Non-Radioactive Cell Proliferation, Promega, Madison, WI) and analyzed at 490 nm. Similarly, hMSC proliferation was examined on graded bioactive scaffolds with nHA concentrations of 20% and 10% of PEG-Da. hMSCs were seeded at 10,000 cells/scaffold and incubated for 1, 3, and 5 days under standard stem cell culture conditions. After rinsing with PBS, the adherent cells were quantified via the MTS assay as previously described.

Confocal microscopy: hMSC 3 and 5 day growth morphology were examined on control and SL printed graded nHA scaffolds. hMSCs were seeded at a density of 50,000 cells and cultured for 3 and 5 days, respectively. The scaffolds were rinsed with PBS 3 times followed by fixation with 4% formaldehyde for 20 min and double-stained with DAPI (cell nucleus) and Texas-Red (actin cytoskeleton), respectively. A ZIESS 710 laser scanning confocal microscope was employed to visualize stem cell spreading morphology.

hMSC chondrogenic and osteogenic differentiation: hMSCs were seeded at a density of 10^5 cells/scaffold for hMSC differentiation. A multilayer scaffold in the absence of morphogenic factors served as a control alongside graded (+20% and 10% nHA / -TGF-β1), blended (+20% and 10% nHA / +bare TGF-β1), and spheres (+20% and 10% nHA / +TGF-β1 nanospheres) experimental groups. Cell seeded scaffolds were cultured in complete media without supplementation of morphogenetic factors for 1 and 2 weeks, respectively. Total DNA content per scaffold was quantified via Quant-iT™ PicroGreen® dsDNA Kit (Invitrogen, Carlsbad, CA). Briefly, a working solution of picogreen reagent in 1x Tris-EDTA buffer was prepared and added at a volume of 100 μL to 100 μL of DNA standard and sample solution in a 96-well plate, respectively. The well plate was read on a fluorescent spectrometer (Spectramax Gemini XPS, Molecular Devices, Sunnyvale, CA) with excitation at 485 nm and emission at 528 nm.

Glycosaminoglycan (GAG), a key component of cartilage matrix, was measured using a standard GAG assay kit (Accurate Chemical & Scientific Corp., Westbury, NY) according to manufacturer's instructions. GAG content was quantified and presented as total GAG content per scaffold. Specifically, a predetermined volume of sample and buffer solution was added to a microcentifuge tube with 500 μL of dye reagent and mixed for 30 minutes. The GAG-dye complex was centrifuged for 10 minutes at 10,000 g until a pellet was visible. The supernatant was decanted and all residual fluid was blotted dry. Next, 600 μL of dissociation reagent was added to the tubes and shaken for 30 minutes; 100 μL of each solution was placed into a 96-well plate and analyzed in triplicate. Absorbance was read at 656 nm and correlated to a standard curve of known standards.

Human type II collagen was evaluated via Type II collagen ELISA (Fisher Scientific, Pittsburgh, PA) per manufacturer's instruction. Briefly, lysed control and sample aliquots were added to pre-coated 96-well plates and incubated. Unbound sample was washed and collagen type II specific detection antibody was added incubated and washed. After washing, tetramethylbenzidine was added producing a color change. The reaction was stopped by the addition of an acidic stop solution and read at 450 nm.

Calcium deposition, one of the most important indicators of osteogenic differentiation, was measured using a calcium reagent kit (Pointe Scientific Inc.). Briefly, hMSCs were lysed through three freeze-thaw cycles and removed. The scaffolds containing deposited calcium and ECM were immersed in a 0.6 N HCl solution at 37°C for 24 h. After the prescribed time period, the amount of dissolved calcium present in the acidic supernatant was measured by reacting with the o-cresolphthalein complexone to form a purple tinted solution. Absorbance was measured by a spectrophotometer at 570 nm. Total calcium deposition was calculated from standard curves of known calcium concentrations run in parallel with experimental groups and normalized to remove contributions associated with incorporated nHA.

Statistical analysis

Data are presented as the mean value ± standard error of the mean (StdEM) and were analyzed via one-way ANOVA and student's t-test to determine differences amongst the groups. Statistical significance was considered at $p<0.05$.

Results

Table-top SL printer design, cure depth analysis, and SL printing of porous scaffolds

The desire to produce complex 3D scaffolds for TE has driven researchers to explore a variety of fabrication technologies. 3D printing techniques, such as SL, are emerging as promising tools for scaffold fabrication. Here, we have developed a novel table-top SL printer to fabricate PEG-based bioactive nanocomposite scaffolds demonstrating the potential for creating multi-material, multi-layered structures. Several aspects of the current system mirror or outperform those of commercial SL systems (such as the Viper si2 SLA rapid prototyping system). The primary benefits include: quick and easy fabrication of multilayered material into a complex structure, lower cost ($10K vs. >$100K), similar spot size (190 ± 50 μm vs. 250 ± 25 μm (normal mode)), and comparable power output (~100 mW). Due to the ability to alter the frequency of the pulsed signal, power at the material's surface can be controlled with a range ~40-110 mW. But, unlike commercial systems, our printer is extremely modular owing to the use of a fiber-optically coupled UV laser source which can be readily fitted with off-the-shelf optics for fine or coarse printing. These results show the great promise of this system for successfully fabricating complex scaffolds using photocrosslinkable hydrogels.

In addition, we have performed initial cure depth studies in an effort to determine optimal printing parameters for adequate interlayer adhesion and resultant scaffold fabrication by examining the effect of print speed and laser frequency. It should be noted that the laser power per unit area for the data in this experiment is ~40 mW/cm^2. Optical images of cure depth samples can be seen in **Figure 2A** with corresponding gel thickness (**Figure 2B**) curves as a function of print speed (mm/min) and laser frequency. For all subsequent studies, a print speed of 2000 mm/min and laser frequency of 5000 Hz was used in order to produce an effective and homogeneous layer thickness of 400 μm when adding 3 mL of nanobioink solution to a 10 cm diameter glass petri dish print substrate. **Figure 3** illustrates the CAD toolpath of the UV laser used in fabricating 15 mm diameter scaffolds of increasing solidity (40%, 60%, and 80%). Optical and SEM analysis (**Figure 3**) show excellent corroboration between the pre-designed porous scaffold and resultant 3D printed structure with excellent horizontal and vertical microchannel formation. Scaffold properties and dimensions of each printed porous structure can be seen in Table 1. Based on the CAD model and SEM analysis, the effective spot size and line width were determined to be ~ 215 µm with discernable high resolution lines for 40% and 60% in-fill density scaffolds. Interestingly, with increased in-fill density (80%) noticeable overlap of lines lead to an effective width of ~ 420 µm. Four-hour hMSC adhesion (**Figure 4**) revealed a statistically significant increase upon 60% in-fill density samples which outperformed low and high in-fill density samples. This can be attributed to the presence of suitable pore size, surface area and porosity when compared to other in-fill densities. For all the following studies, an in-fill density of 60% was used.

Nanobioink characterization and bioactive graded osteochondral scaffold fabrication

Morphological analysis of synthesized nHA displayed grain sizes in the range of 80-100 nm (**Figure 5A**) in length and PLGA nanospheres (**Figure 5B)** on the order of 75 ± 17 nm in diameter. Based on the ease by which the composition of each layer can be altered, the table-top SL printer was used to 3D print a three-layer graded osteochondral scaffold exhibiting a solid articular cartilage layer and 10% and 20% nHA middle and bottom layer to serve as the calcified transitional zone and subchondral region. **Figures 6A-C** show the CAD model design of the 3D graded osteochondral scaffold. Retention of printability is evident upon SEM evaluation (**Figure 6**) of scaffold morphology. In addition, SEM image analysis (**Figures 6H-I**) reveals a more biomimetic scaffold with respect to nanotexturization and bioactivity in the presence of 10% and 20% nHA when compared to the controls, as well as aids in enhancing the compressive strength of the overall scaffold (**Figure 7**). A 29% increase in compressive modulus was observed in the graded osteochondral scaffold when compared to non-nHA control.

In addition to enhanced compressive strength, a five-day hMSC proliferation study was performed (**Figure 8**). With the incorporation of nHA nanoparticles, a more than 20% increase in cell density was observed after 3 day culture. In addition, as shown in **Figure 9,** three and five-day hMSC spreading morphology on 3D printed graded scaffolds containing spatially distributed nHA was greatly enhanced when compared to controls. After three days of culture, hMSCs display excellent spreading when compared to the spherical morphology of hMSCs seeded upon control scaffolds which can be correlated to an increase in nanotexturization and resultant increase in surface area.

Furthermore, a growth factor release study was conducted to determine TGF-β1 release kinetics of the nanocomposite osteochondral scaffold developed here. **Figure 10** shows the cumulative release profiles of bare TGF-β1 and TGF-β1 encapsulated nanospheres within a graded scaffold. Both scaffolds can sustainably release growth factors over 14 days. In particular, the PLGA nanosphere-containing scaffolds exhibited further inhibited initial burst release and steady TGF-β1 delivery over 14 days when compared non-nanosphere samples. In addition, due to the extreme flexibility of the co-axial system, a wide range of polymers can be readily used as encapsulants for sustained delivery.

Enhanced hMSC chondrogenic and osteogenic differentiation upon bioactive graded osteochondral scaffolds containing osteogenic nHA and chondrogenic TGF-β1 nanospheres

For hMSC osteochondral differentiation studies, the bioactive osteochondral scaffold was evaluated for chondrogenic and osteogenic differentiation potential, respectively. Seeded samples were evaluated for total DNA content, GAG, type II collagen, and extracellular calcium deposition after two weeks of culture. **Figure 11** shows total DNA content corresponding to cell number per scaffold. There is no significant difference of hMSC density amongst the sample groups.

Figure 12 showed a significant increase in GAG production upon TGF-β1 incorporated scaffolds (blended) at week 2 when compared to controls. All nHA-containing scaffolds exhibited a significant increase in GAG production after two weeks when compared to week 1. Graded scaffolds yielded a 90% increase with bare TGF-β1 inducing a 78% increase and PLGA nanosphere containing samples outperforming all other sample groups with an increase of 126% from week 1 to week 2. In addition, **Figure 13** illustrates another important cartilage matrix protein--type II collagen synthesis in bioactive graded osteochondral scaffolds. As a late-stage marker of chondrogenic differentiation, type II collagen synthesis showed 25%-30% increases after two weeks for TGF-β1 encapsulated nanosphere scaffolds when compared to control and all other experimental groups.

In addition to improved chondrogenic differentiation, our osteochondral scaffold with nHA and TGF-β1 are promising for enhanced osteogenic differentiation of hMSCs. In particular, deposited extracellular calcium results (**Figure 14**) revealed greater calcium deposition amongst graded and TGF-β1 encapsulated nanosphere-containing samples after one week of culture when compared to control. After two weeks, all sample groups displayed enhanced extracellular calcium deposition when compared to control. Both, graded and nanosphere containing nanocomposite scaffolds, exhibited increased extracellular calcium deposition of 17% and 18% after one week and a 20% and 22% increase after 2 weeks culture, respectively, when compared to control. Taken collectively, all of the above data reveal the great potential of this novel 3D printing system and graded bioactive nanocomposite scaffold for efficient delivery of TGF-β1, creating nano surface topography and subsequent improved growth, chondrogenic/osteogenic differentiation of hMSCs.

Discussion

Table-top SL printing for the fabrication of bioactive graded nanocomposite scaffolds with sustained bioactive factor delivery

The novel 3D printing system developed here allows for the rapid fabrication of photocrosslinkable hydrogel scaffolds with efficient and effective incorporation of nanobiomaterials leading to increased nanoscale surface roughness and highly porous geometry. In addition, modifications to the 3D model can be readily made where each respective layer's in-fill density (corresponding to pore density) and orientation can be readily controlled creating a gradual transition of bioactivity and geometry. The composition of the 3D printed scaffold can be customized to regenerate a particular tissue type through the incorporation of tissue-specific organic and inorganic components in a highly reproducible manner.

Surface topography is an important feature when designing scaffolds for tissue engineering applications.[37] The 3D osteochondral scaffold developed here integrated bioactive inorganic nano ceramics and nanosphere growth factor delivery for a cell-favorable surface topography. Specifically, one of the key nanomaterials utilized in the manufacture of our graded osteochondral scaffold, nHA, can provide several key benefits to include: mechanical reinforcement, nanotexturization, and osteoconductivity. As a bioactive and osteoconductive chemical component in bone and the calcified zone in cartilage,[38-40] hydroxyapatite and its chemical derivatives have been extensively studied and shown to increase cell-scaffold performance via incorporation within a bulk matrix[3] as well as surface adsorption[41-43] and *in situ* nucleation.[44-46] Through a hydrothermal treatment method, our lab readily synthesizes biomimetic nHA with excellent control of nano scale crystallinity and surface morphology. Our hydrothermally treated nHA serves as an excellent mechanical reinforcer within our 3D printed osteochondral construct. Furthermore, the capacity of 3D printed scaffolds to withstand compressive loads is important due to the fact that human osteochondral tissue in joints is under repetitive compressive loading on a daily basis. Tissue degeneration emanating from injuries to the cartilage layer is largely exacerbated by mismatches in implant-host tissue stiffness. The scaffolds fabricated here display compressive strength similar to that of native osteochondral tissue and other reported biphasic systems therefore rendering the fabricated scaffold less likely to fail.[47]

In addition, the incorporation of PLGA nanospheres was employed as a sustained delivery device which promoted synergistic interactions when combined with other incorporated nanobiomaterials as evidenced by controlled and sustained bioactive factor delivery. It is well known that various growth factors (e.g., TGF-β1) have been shown to improve hMSC osteogenic and chondrogenic differentiation.[48-50] Unfortunately, for *in vivo* applications, these growth factors face ongoing issues related to short-term retention, quick half-life in circulation, and quick loss of biological activity even when administered at high doses. Therefore, we extended the application of the scaffold design to not only serve as a 3D structural support for cellular attachment, but as a sustained TGF-β1 delivery device for long-term osteochondral tissue regeneration. A significant decrease in growth factor release was observed and is postulated to be attributed to differences in biomaterial degradation where low molecular weight PEGs degrade at a quicker rate than PLGA-based polymers.[51, 52] Therefore, by utilizing PLGA as the nanosphere material, inhibited degradation can be achieved. In addition, electrostatic interactions amongst the negative carboxyl terminals of the globular protein and positively-charged species (H^+ and Ca^{2+}) of the nHA particles present at the material's surface[53] as well as electrostatic interactions of the bulk hydrogel matrix may also contribute retention of growth factor.

Enhanced hMSC function and osteochondral matrix development within 3D printed bioactive graded scaffolds

Scaffolds with a highly interconnected microporous calcified transitional and subchondral region were created which facilitated cell adhesion, proliferation, and cellular activities. The selected 3D printed scaffolds with 60% in-filling density outperformed scaffolds with larger pores. This porous structure allows for efficient exchange of nutrients and metabolic waste removal during new tissue formation. Through the incorporation of osteoconductive nHA, hMSC growth was enhanced. Our cell studies confirmed that the synthesized nHA can be an excellent osteoconductive chemical cue for improving hMSC proliferation and early osteogenesis *in vitro.* Qualitative evaluation of hMSC growth morphology reveal increased cell density and excellent cell spreading as noted by the extension of filopodia.

The notable increase in GAG production upon TGF-β1 containing samples is postulated to be directly related to sustained growth factor release and synergetic interactions of growth factor and nHA particles. Bare TGF-β1 samples lead to increased GAG production after two weeks of culture as illustrated by decreased release kinetics. Tezcan et al.[54] revealed a dose-dependent response of TGF-β1 induced hMSC chondrogenic differentiation wherein TGF-β1 was critical in the initiation of GAG synthesis and late stage tissue maturation. Although TGF-β1 was added only to the top cartilage layer, localized diffusion through the entire construct is facilitated by the inherent microporous nature of the PEG-Da hydrogel whose composition consisted of a 40% soluble fraction as characterized in our previous work.[3] In addition, type II collagen and extracellular calcium deposition increased upon PLGA nanosphere scaffolds providing further evidence of bioactive nanosphere upon improving osteochondral tissue formation. Based on more favorable surface topography, steric interactions of biological constituents in the presence of PLGA nanospheres when compared to hydrogel alone in concert with extended release may lead to expedited tissue formation as evident by the increase in late-stage ECM markers.

Conclusions:

The work presented herein served to illustrate the efficacy of the nano-ink and current table-top SL 3D printing technology for efficient fabrication of a novel graded nanocomposite osteochondral scaffold with predesigned micro architecture and controlled factor release. hMSC proliferation, and osteochondral differentiation were greatly enhanced through the incorporation of tissue-specific nHA and TGF-β1 encapsulated nanospheres. Moreover, due to the flexible design nature of our printing system and CAD modeling, a variety of complex tissue or even organ scaffolds with nanomaterials and growth factors can be readily fabricated, thus make them promising for diverse tissue and organ regeneration applications.

Acknowledgements

The authors would like to thank NIH Director’s New Innovator Award (DP2EB020549) and GW Institute for Biomedical Engineering for financial support.

Notes and references

1. G. W. Tang, H. Zhang, Y. H. Zhao, Y. Zhang, X. L. Li and X. Y. Yuan, *J Biomat Sci-Polym E*, 2012, **23**, 2241-2257.
2. P. Sibilla, A. Sereni, G. Aguiari, M. Banzi, E. Manzati, C. Mischiati, L. Trombelli and L. del Senno, *J Dent Res*, 2006, **85**, 354-358.
3. N. J. Castro, C. M. O'Brien and L. G. Zhang, *Aiche J*, 2014, **60**, 432-442.
4. X. Z. Zhou, V. Y. Leung, Q. R. Dong, K. M. Cheung, D. Chan and W. W. Lu, *Int J Artif Organs*, 2008, **31**, 480-489.
5. J. I. Dawson, D. A. Wahl, S. A. Lanham, J. M. Kanczler, J. T. Czernuszka and R. O. Oreffo, *Biomaterials*, 2008, **29**, 3105-3116.
6. I. O. Smith, X. H. Liu, L. A. Smith and P. X. Ma, *Wiley Interdisciplinary Reviews-Nanomedicine and Nanobiotechnology*, 2009, **1**, 226-236.
7. T. Weigel, G. Schinkel and A. Lendlein, *Expert Rev Med Devic*, 2006, **3**, 835-851.
8. S. Lin-Gibson, J. A. Cooper, F. A. Landis and M. T. Cicerone, *Biomacromolecules*, 2007, **8**, 1511-1518.
9. T. S. Karande, J. L. Ong and C. M. Agrawal, *Annals of Biomedical Engineering*, 2004, **32**, 1728-1743.
10. D. W. Hutmacher, *J Biomat Sci-Polym E*, 2001, **12**, 107-124.
11. A. Vats, N. S. Tolley, J. M. Polak and J. E. Gough, *Clinical Otolaryngology*, 2003, **28**, 165-172.
12. V. Karageorgiou and D. Kaplan, *Biomaterials*, 2005, **26**, 5474-5491.
13. C. Erisken, D. M. Kalyon and H. Wang, *Biomaterials*, 2008, **29**, 4065-4073.
14. C. Erisken, D. M. Kalyon and H. Wang, *Nanotechnology*, 2008, **19**, 165302.
15. S. Ozkan, D. M. Kalyon and X. Yu, *J Biomed Mater Res A*, 2010, **92**, 1007-1018.
16. S. Ozkan, D. M. Kalyon, X. Yu, C. A. McKelvey and M. Lowinger, *Biomaterials*, 2009, **30**, 4336-4347.
17. A. Ergun, X. Yu, A. Valdevit, A. Ritter and D. M. Kalyon, *J Biomed Mater Res A*, 2011, **99**, 354-366.
18. A. Ergun, X. Yu, A. Valdevit, A. Ritter and D. M. Kalyon, *Tissue engineering. Part A*, 2012, **18**, 2426-2436.
19. C. O'Brien, B. Holmes, S. Faucett and L. G. Zhang, *Tissue Eng Part B Rev*, 2015, **21**, 103-114.
20. B. Holmes, W. Zhu, J. Li, J. D. Lee and L. G. Zhang, *Tissue Eng Part A*, 2015, **21**, 403-415.
21. S. Ichinose, K. Yamagata, I. Sekiya, T. Muneta and M. Tagami, *Clin Exp Pharmacol Physiol*, 2005, **32**, 561-570.
22. W. G. Bian, D. C. Li, Q. Lian, X. Li, W. J. Zhang, K. Z. Wang and Z. M. Jin, *Rapid Prototyping J*, 2012, **18**, 68-80.
23. S. V. Murphy, A. Skardal and A. Atala, *J Biomed Mater Res A*, 2013, **101A**, 272-284.
24. N. J. Castro, R. Patel and L. Zhang, *Cellular and Molecular Bioengineering*, 2015, 1-17.
25. L. Zhang and T. J. Webster, *Nano Today*, 2009, **4**, 66-80.
26. A. Baji, S. C. Wong, T. S. Srivatsan, G. O. Njus and G. Mathur, *Mater Manuf Process*, 2006, **21**, 211-218.
27. D. G. Marchesi, *Eur Spine J*, 2000, **9**, 372-378.
28. C. Piconi and G. Maccauro, *Biomaterials*, 1999, **20**, 1-25.
29. C. D. Friedman, P. D. Costantino, S. Takagi and L. C. Chow, *Journal of Biomedical Materials Research*, 1998, **43**, 428-432.

30. I. Sopyan, M. Mel, S. Ramesh and K. A. Khalid, *Science and Technology of Advanced Materials*, 2007, **8**, 116-123.
31. Y. K. Hwang, U. Jeong and E. C. Cho, *Langmuir*, 2008, **24**, 2446-2451.
32. O. Im, J. Li, M. Wang, L. G. Zhang and M. Keidar, *Int J Nanomedicine*, 2012, **7**, 2087-2099.
33. M. Wang, N. J. Castro, J. Li, M. Keidar and L. G. Zhang, *J Nanosci Nanotechno*, 2012, **12**, 7692-7702.
34. L. Zhang, Y. Chen, J. Rodriguez, H. Fenniri and T. J. Webster, *International Journal of Nanomedicine*, 2008, **3**, 323-333.
35. L. Zhang, J. Rodriguez, J. Raez, A. J. Myles, H. Fenniri and T. J. Webster, *Nanotechnology*, 2009, **20**, 175101.
36. L. Sun, L. Zhang, U. D. Hemraz, H. Fenniri and T. J. Webster, *Tissue engineering. Part A*, 2012, **18**, 1741-1750.
37. E. S. Place, J. H. George, C. K. Williams and M. M. Stevens, *Chemical Society reviews*, 2009, **38**, 1139-1151.
38. L. Zhang and T. J. Webster, *Nanotoday*, 2009, **4**, 66-80.
39. L. Zhang, S. Sirivisoot, G. Balasundaram and T. J. Webster, in *Advanced Biomaterials: Fundamentals, Processing and Application*, eds. B. Basu, D. Katti and A. Kuma, John Wiley & Sons Inc., New Jersey, 2009, pp. 205-241.
40. J. Li, J. D. Lee and K. P. Chong, *International Journal of Smart and Nano Materials*, 2011, **3**, 2-13.
41. D. Moreau, A. Villain, D. N. Ku and L. Corte, *Biomatter*, 2014, **4**, e28764.
42. K. Matsumura, T. Hayami, S. H. Hyon and S. Tsutsumi, *J Biomed Mater Res A*, 2010, **92**, 1225-1232.
43. K. Madhumathi, K. T. Shalumon, V. V. Rani, H. Tamura, T. Furuike, N. Selvamurugan, S. V. Nair and R. Jayakumar, *International journal of biological macromolecules*, 2009, **45**, 12-15.
44. L. C. Wu, J. Yang and J. Kopecek, *Biomaterials*, 2011, **32**, 5341-5353.
45. A. Sugino, T. Miyazaki and C. Ohtsuki, *Journal of materials science. Materials in medicine*, 2008, **19**, 2269-2274.
46. T. Iwatsubo, K. Sumaru, T. Kanamori, T. Shinbo and T. Yamaguchi, *Biomacromolecules*, 2006, **7**, 95-100.
47. L. Zhang, J. Hu and K. A. Athanasiou, *Crit Rev Biomed Eng*, 2009, **37**, 1-57.
48. H. Chim, E. Miller, C. Gliniak and E. Alsberg, *Cell Tissue Res*, 2012, **350**, 89-94.
49. M. Kim, I. E. Erickson, M. Choudhury, N. Pleshko and R. L. Mauck, *J Mech Behav Biomed Mater*, 2012, **11**, 92-101.
50. A. B. Ertan, P. Yilgor, B. Bayyurt, A. C. Calikoglu, C. Kaspar, F. N. Kok, G. T. Kose and V. Hasirci, *Journal of tissue engineering and regenerative medicine*, 2011, DOI: 10.1002/term.509.
51. H. K. Makadia and S. J. Siegel, *Polymers*, 2011, **3**, 1377-1397.
52. S. P. Zustiak and J. B. Leach, *Biomacromolecules*, 2010, **11**, 1348-1357.
53. S. Tarafder, S. Banerjee, A. Bandyopadhyay and S. Bose, *Langmuir*, 2010, **26**, 16625-16629.
54. B. Tezcan, S. Serter, E. Kiter and A. C. Tufan, *Journal of molecular histology*, 2010, **41**, 247-258.

Table 1. Dimensions and parameters of table-top SL 3D printed porous scaffolds

In-fill Density	Surface Area	Volume	% Porosity	SA/V Ratio	Line Width	Max Pore Size
40%	408.9 mm^2	28.1 mm^3	79.6	14.6	215 µm	1250 µm
60%	613.8 mm^2	42.3 mm^3	69.3	14.5	215 µm	790 µm
80%	718.3 mm^2	71.4 mm^3	48.2	10.1	420 µm	500 µm

List of Figures:

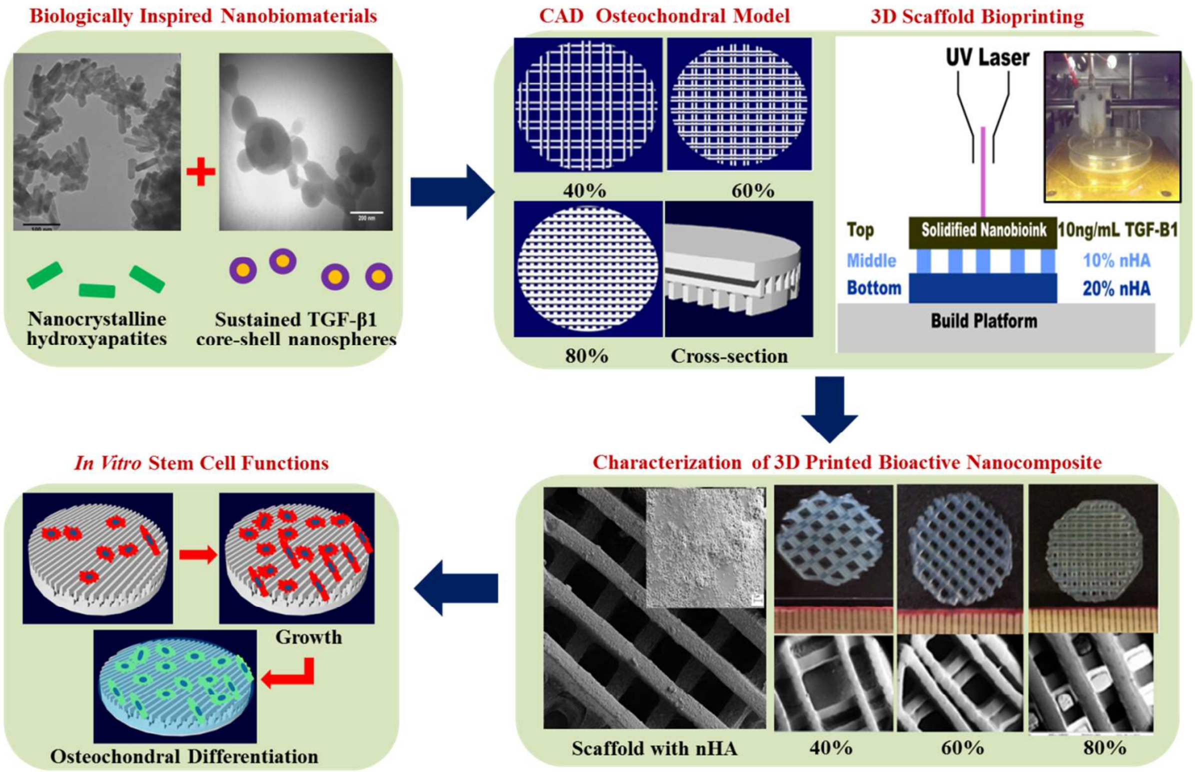

Figure 1. A flow chart of SL printed biomimetic nanocomposite osteochondral scaffold. Tissue-specific nanomaterials for osteogenic (nHA) and chondrogenic (TGF-β1 loaded PLGA nanospheres) differentiation of hMSCs. CAD model of porous scaffold design and composition. 3D printed bioactive scaffolds via table-top SL and *in vitro* hMSC studies.

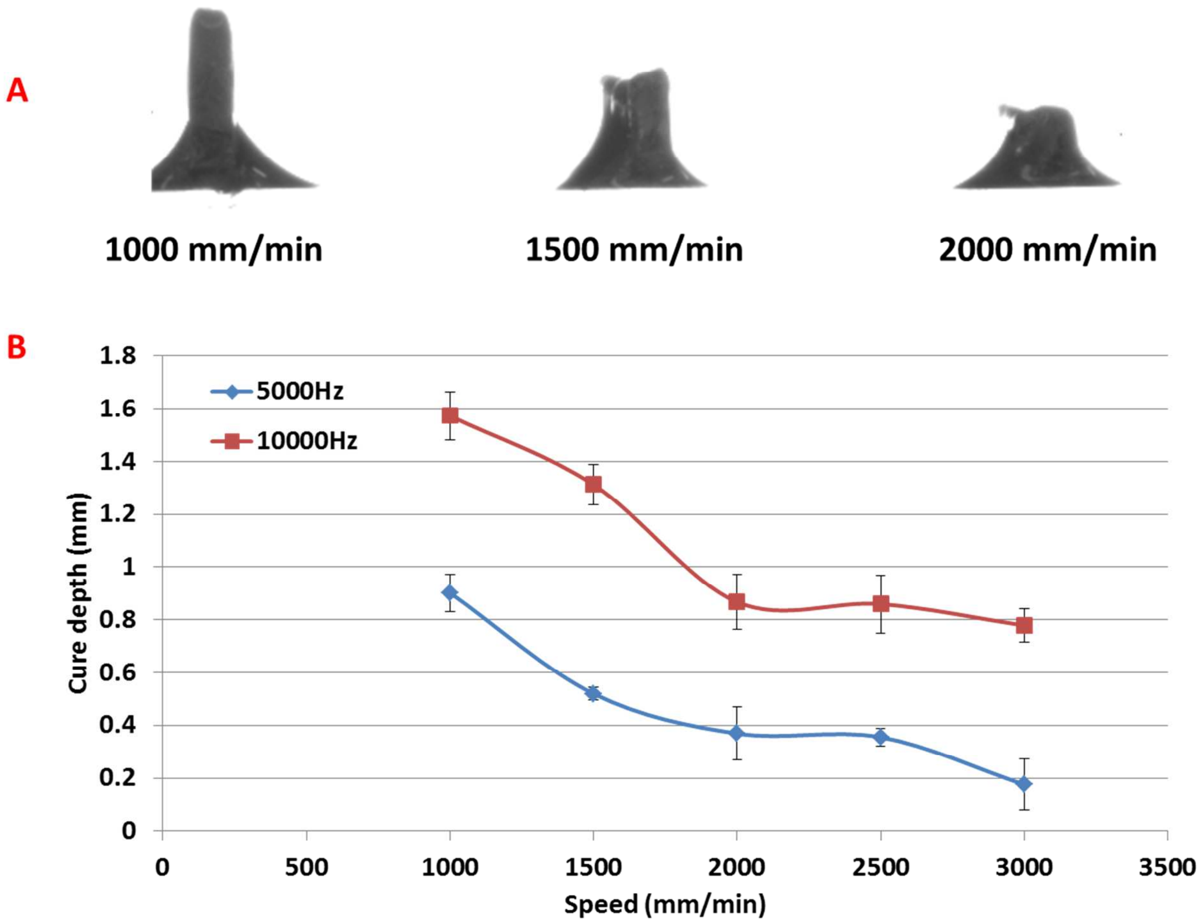

Figure 2. Optical micrograph (A) of cure depth samples at 5000 Hz and cure depth plot (B) of pulsed laser UV crosslinking of 60% PEG-Da/PEG (wt%) at 5000 Hz and 10000 Hz.

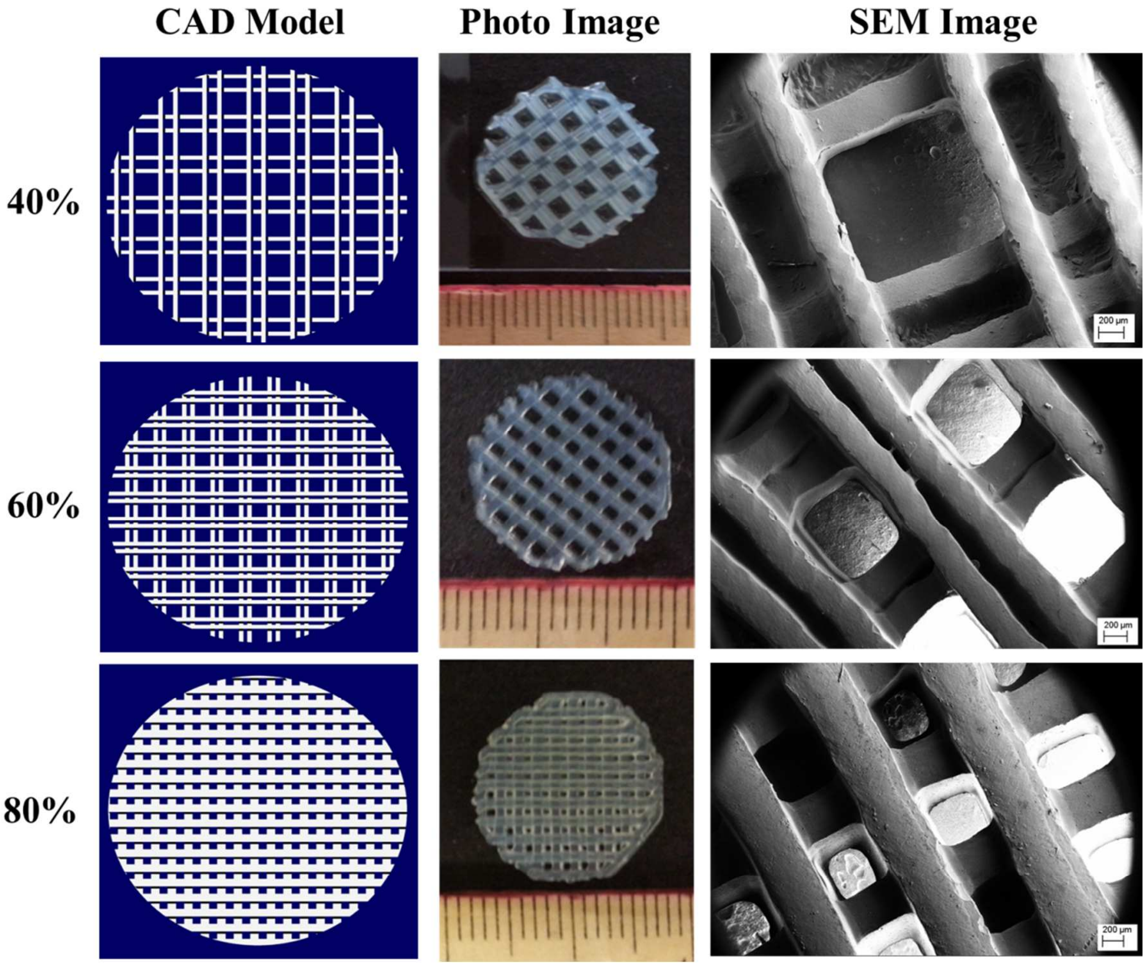

Figure 3. CAD models, optical, and scanning electron micrographs of hydrogel scaffolds with varying in-fill densities.

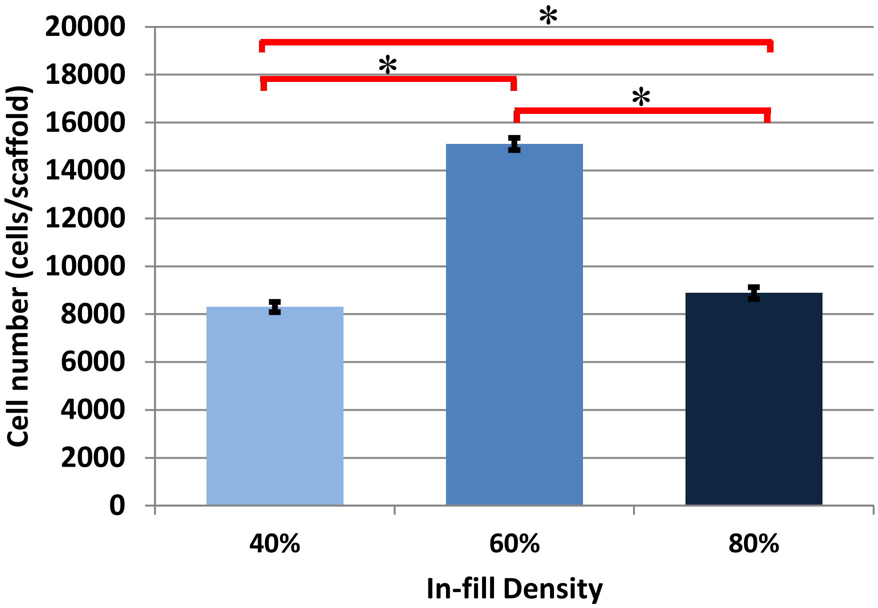

Figure 4. 4-hour hMSC adhesion on 3D printed hydrogel scaffolds of varying in-fill densities (Data are mean ± StdEM, N = 3, *p < 0.05).

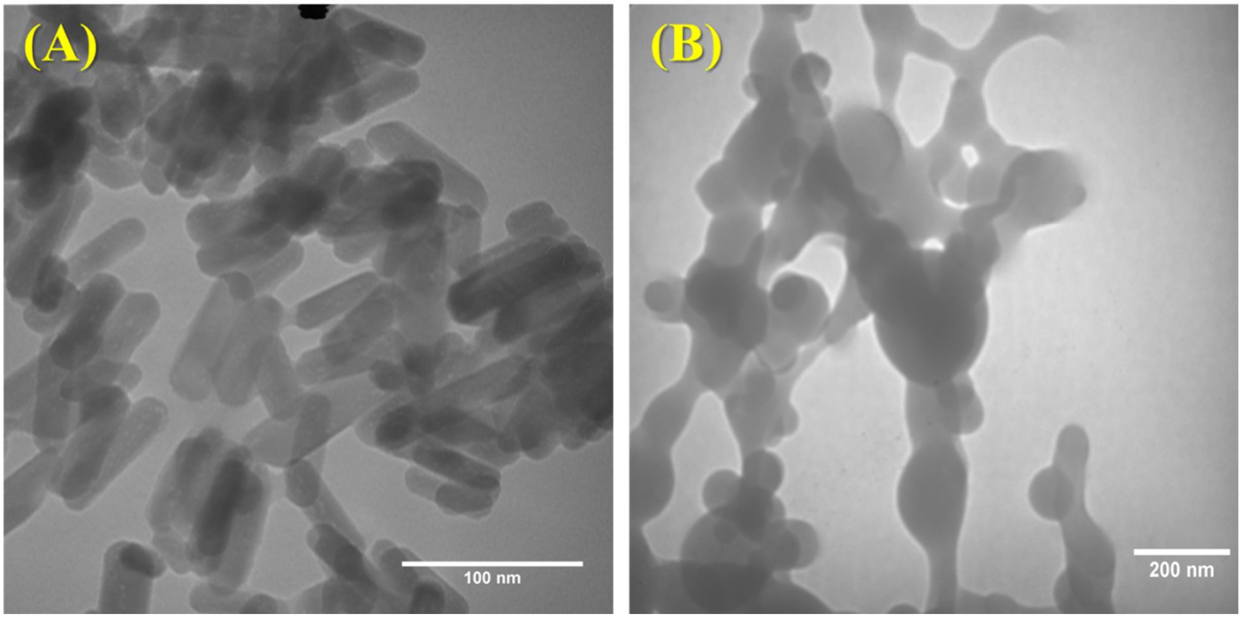

Figure 5. TEM images of (A) hydrothermally treated nHA and (B) TGF-β1 encapsulated nanospheres.

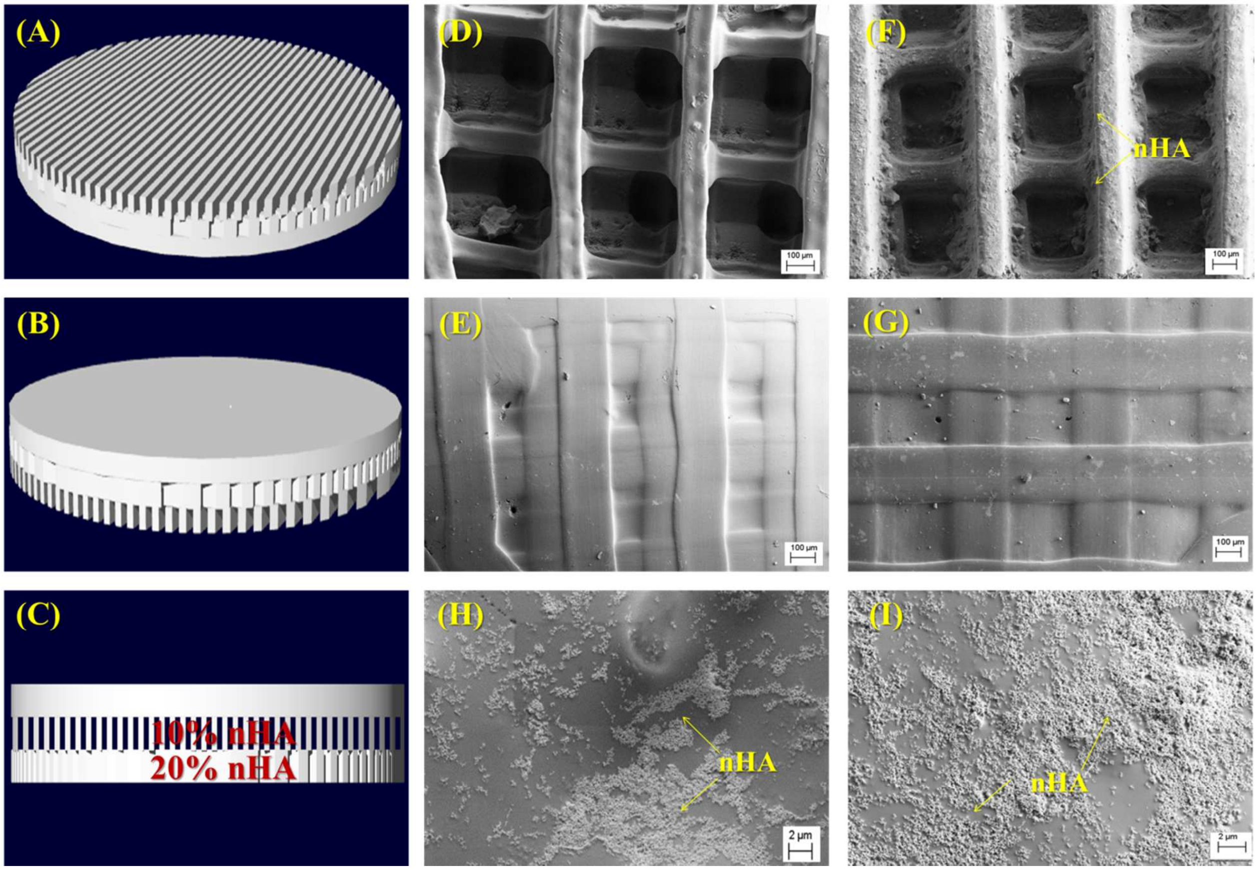

Figure 6. (A-C) 3D CAD model (bottom, top and side view) of the three-layer osteochondral scaffold design with 60% in-fill density. SEM images of (D-E) control scaffolds without nHA (bottom and top images); and (F-I) osteochondral scaffolds with graded nHA (F is the bottom, G is the top; H is 10% nHA layer and I is 20% nHA layer).

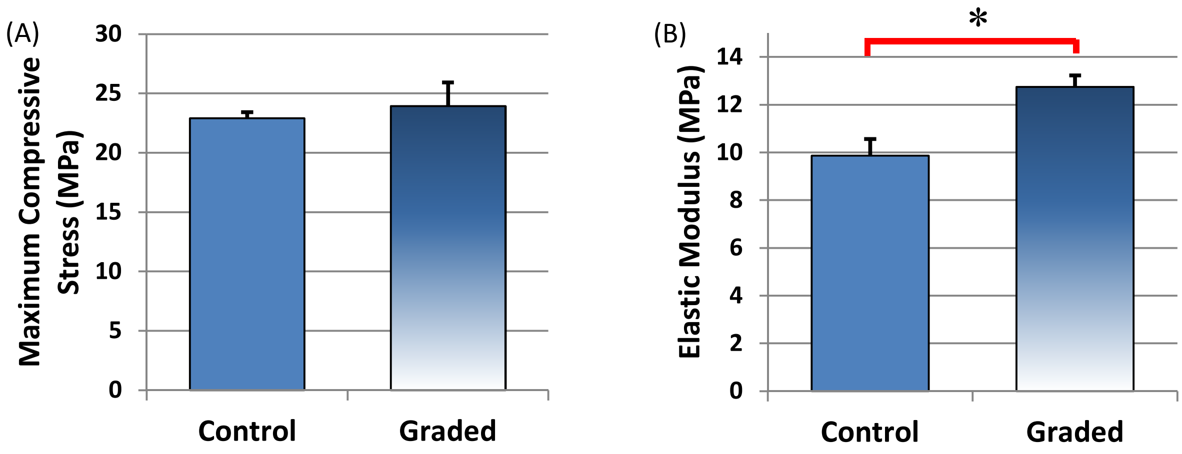

Figure 7. Uniaxial compression testing of three-layer 3D printed control and graded nHA scaffolds. Graded scaffolds display (A) a similar max load and (B) a 29% increase in elastic modulus when compared to control. (Data are mean ± StdEM, n = 5, $*p < 0.05$).

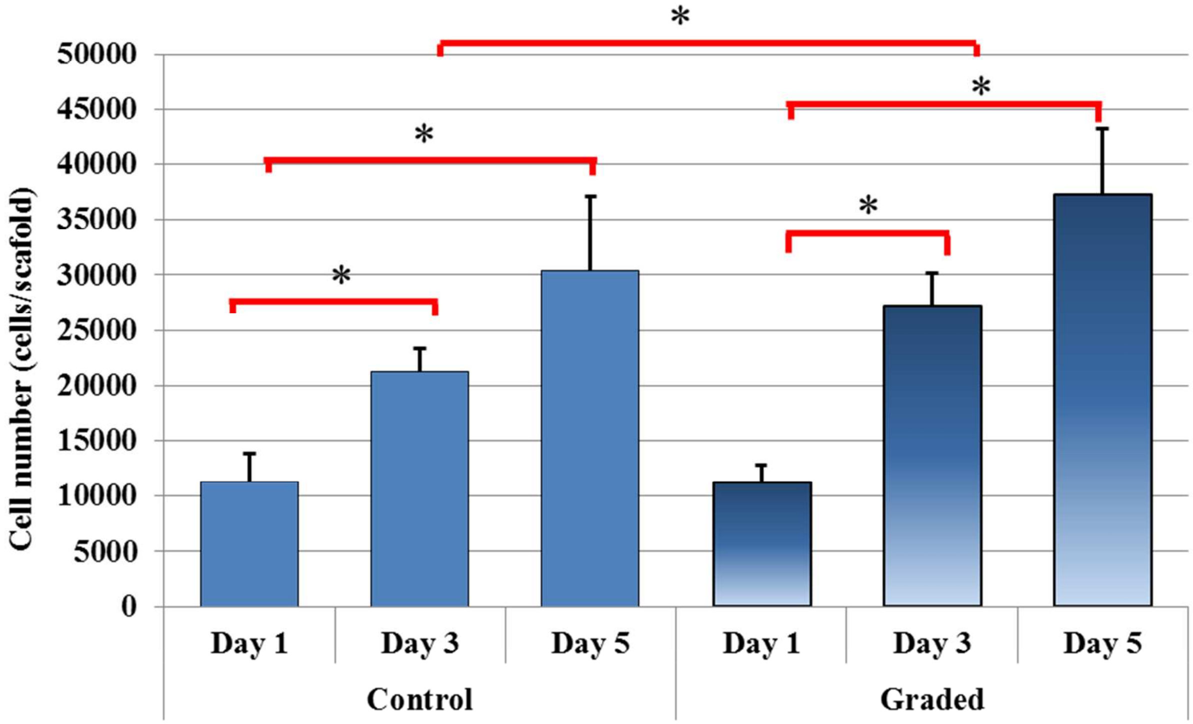

Figure 8. Five-day hMSC proliferation on 3D printed osteochondral scaffolds containing spatially distributed nHA. (Data are mean ± StdEM, N = 3, $^{*}p < 0.05$).

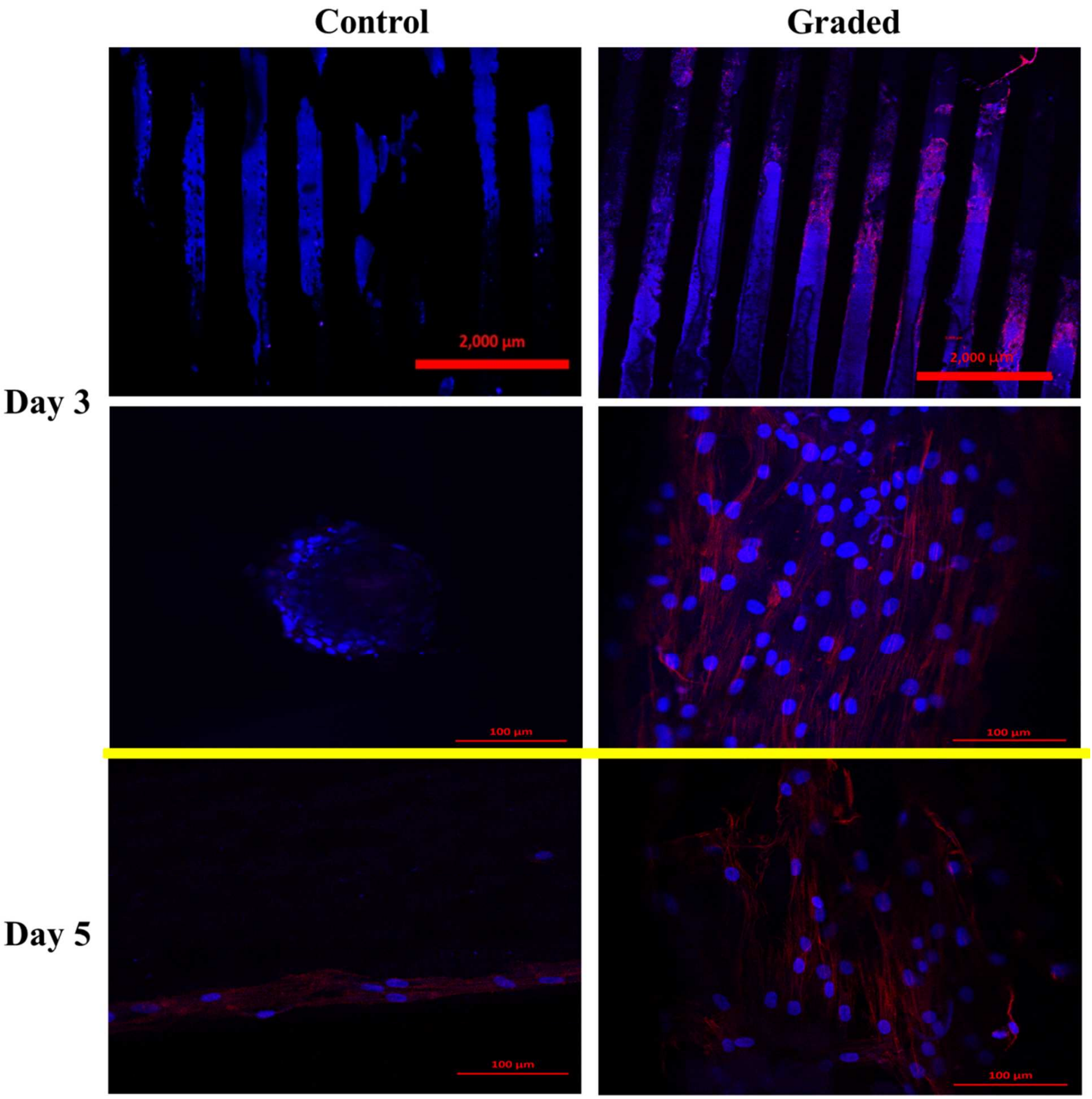

Figure 9. Three and five-day hMSC spreading morphology on 3D printed scaffolds containing spatially distributed nHA (graded) when compared to controls. After three days of culture, hMSCs display excellent spreading when compared to the spherical morphology of hMSCs seeded upon control scaffolds. In addition, increased cell growth density can be seen as illustrated through DAPI staining of cell nuclei.

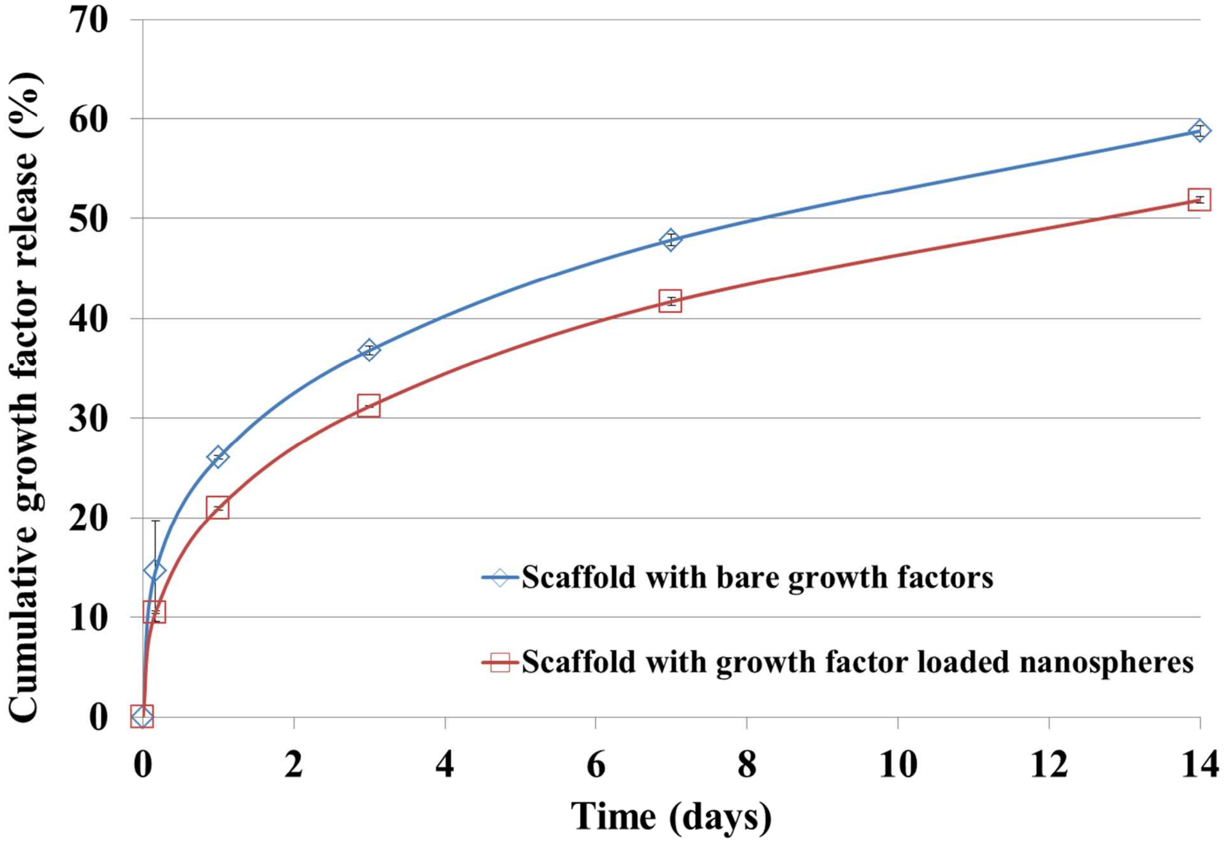

Figure 10. Two-week TGF-β1 release study of blended and nanosphere encapsulated growth factors within the articulating cartilage layer of graded nHA scaffolds. (Data are mean ± StdEM, n = 3).

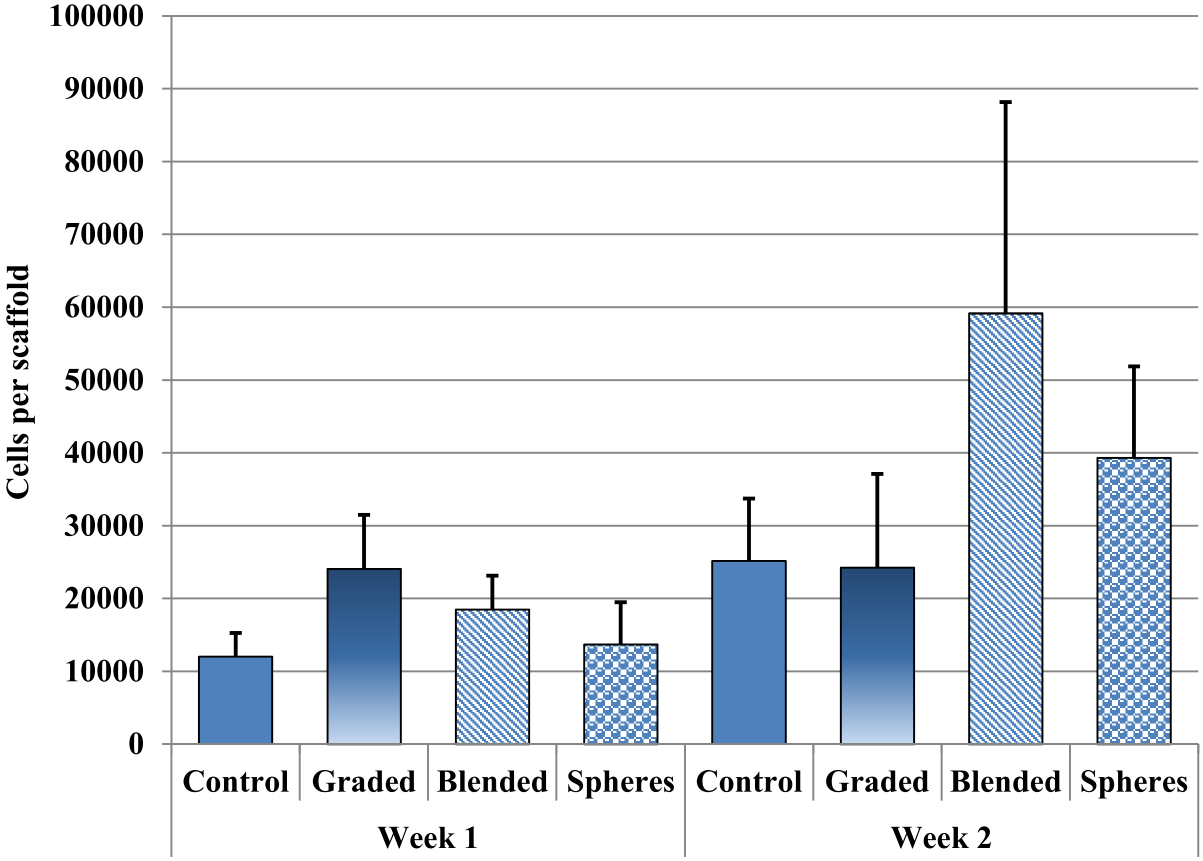

Figure 11. Two-week total DNA content of hMSC seeded control, graded, and TGF-β1 incorporated osteochondral scaffolds. (Data are mean ± StdEM, N = 3).

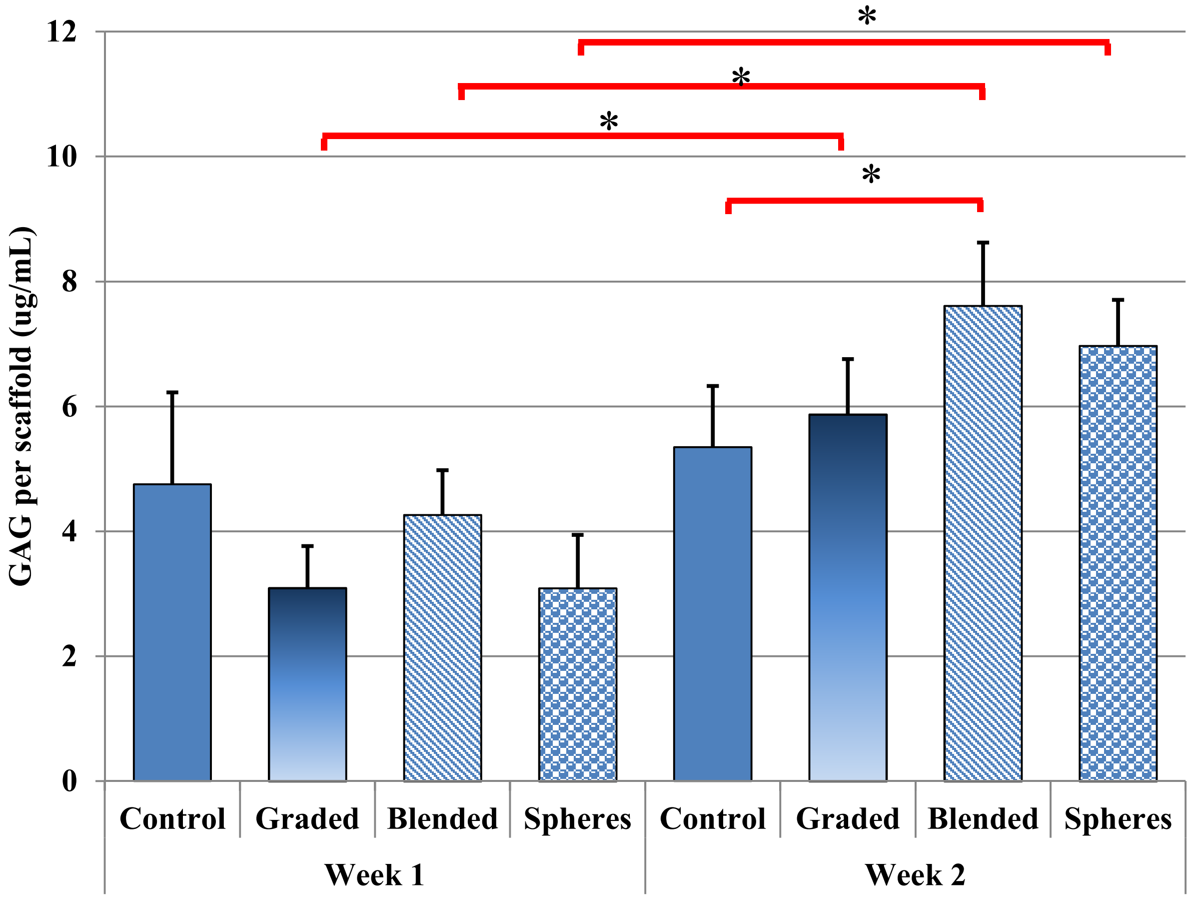

Figure 12. Two-week hMSC GAG production. All nHA containing scaffolds at week 2 showed a significant increase in GAG production when compared to week 1. (Data are mean ± StdEM, N = 3, $*p < 0.05$).

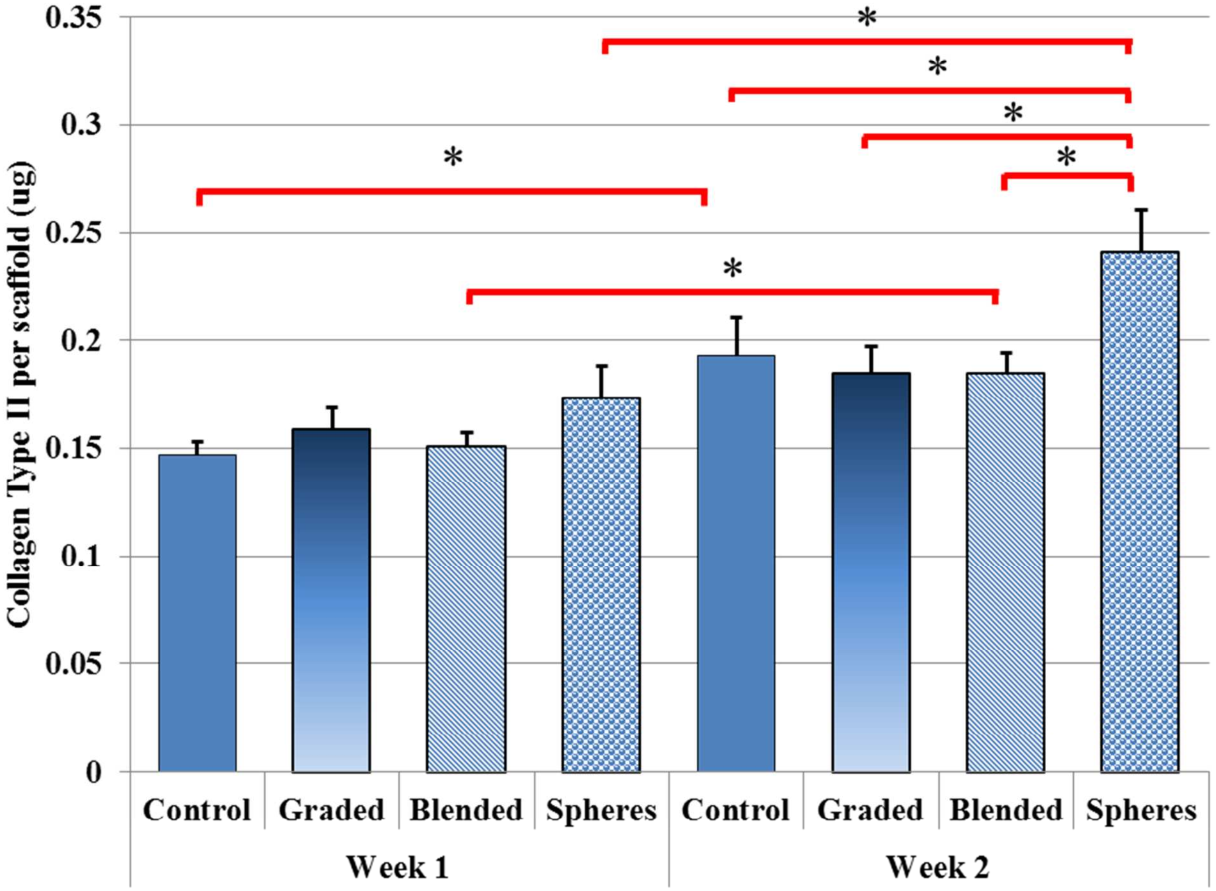

Figure 13. Two-week hMSC collagen type II production. TGF-β1 encapsulated nanospheres incorporated within graded nHA scaffolds showed the greatest collagen production after two weeks when compared to all other groups. (Data are mean ± StdEM, N = 3, $^*p < 0.05$).

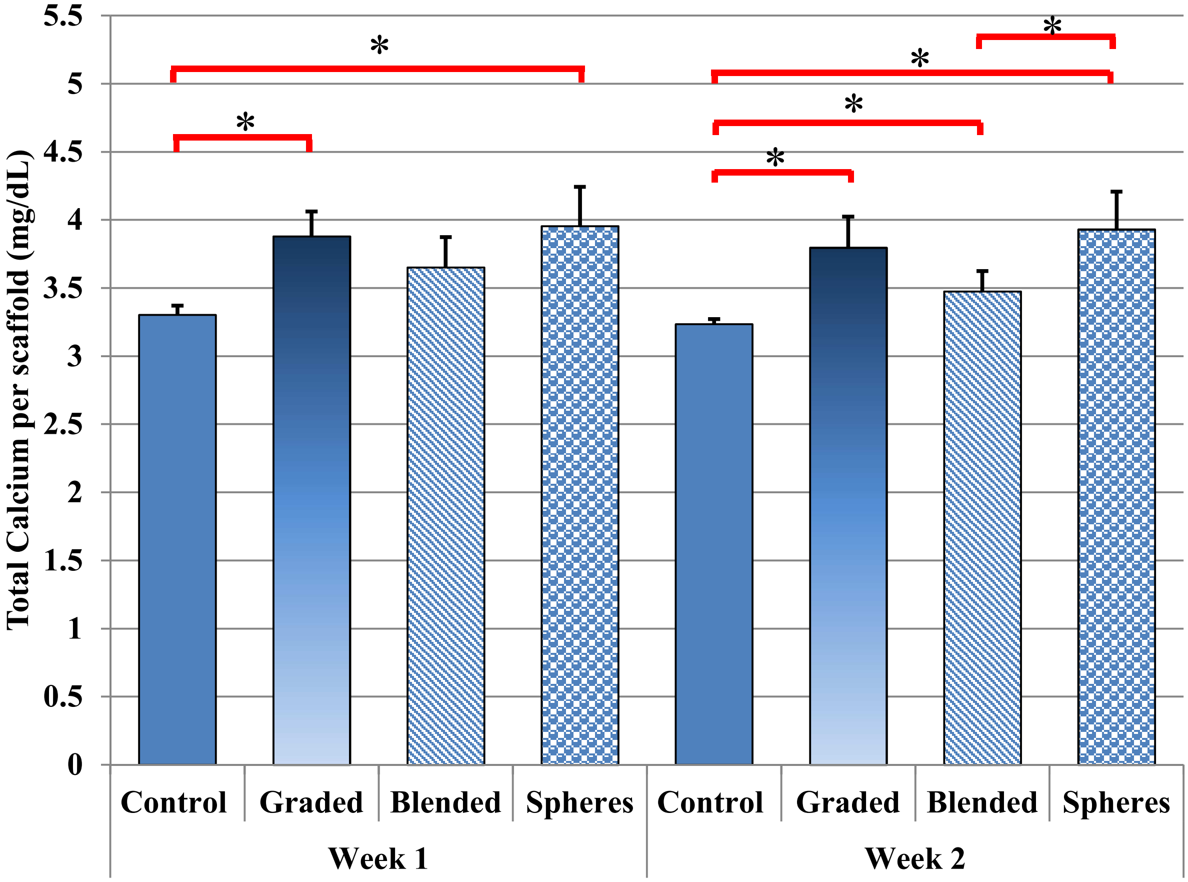

Figure 14. Two-week hMSC total calcium deposition. nHA containing scaffolds showed an increase in total extracellular calcium deposition after one and two weeks of culture when compared to control. TGF-β1 encapsulated nanospheres incorporated within graded nHA scaffolds showed the greatest extracellular calcium deposition after two weeks. (Data are mean ± StdEM, N = 3, *$p < 0.05$).